Cell

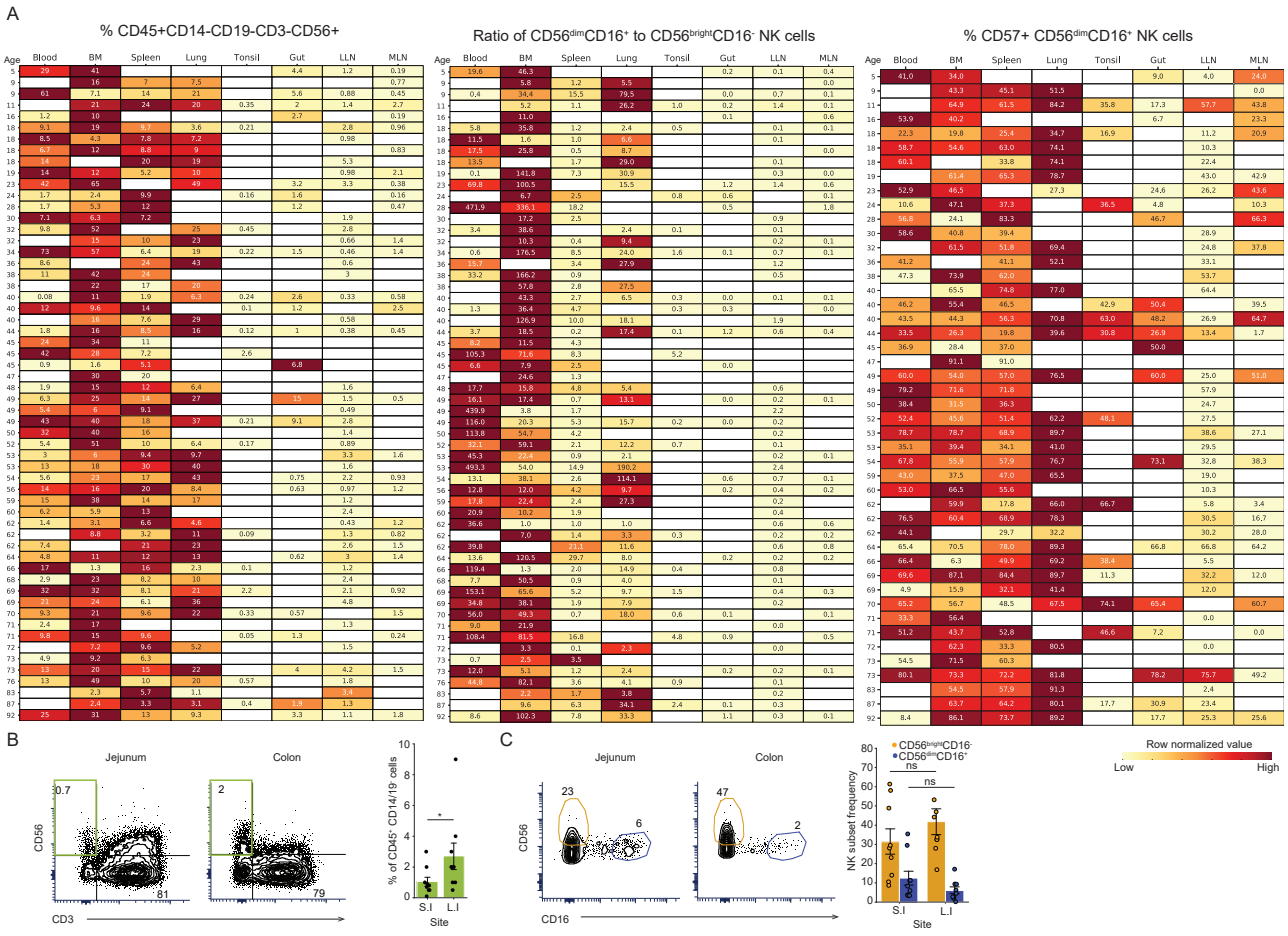

Figure S1. NK Cell and Subset Distribution in Different Tissue Sites, Related to Figure 1

(A) Heatmaps showing frequency of NK cells (left), ratio of $CD56^{dim}CD16^{+}$ to $CD56^{bright}CD16^{-}$ NK cells (middle) and frequency of $CD57^{+}CD56^{dim}CD16^{+}$ NK cells in blood and tissue sites for each individual donor reported in this study. Donors are arranged by increasing age and color intensity of each cell is based on row normalization of (min-max scaled) values. White cells indicate that no sample was obtained for a given donor.

(B) Representative flow plots showing NK cell frequency (top left quadrant) in small and large intestine sites reported in this study on left, and on right bar plots showing data compiled from 9 donors.

(C) Representative flow plots showing NK cell subset frequency in small and large intestine sites reported in this study on left, and on right bar plots showing data compiled from 9 donors.

Error bars represent ± SEM, *p $\leq$ 0.05; ns, non-significant. BM, bone marrow; LLN, lung draining LN; MLN, mesenteric LN.

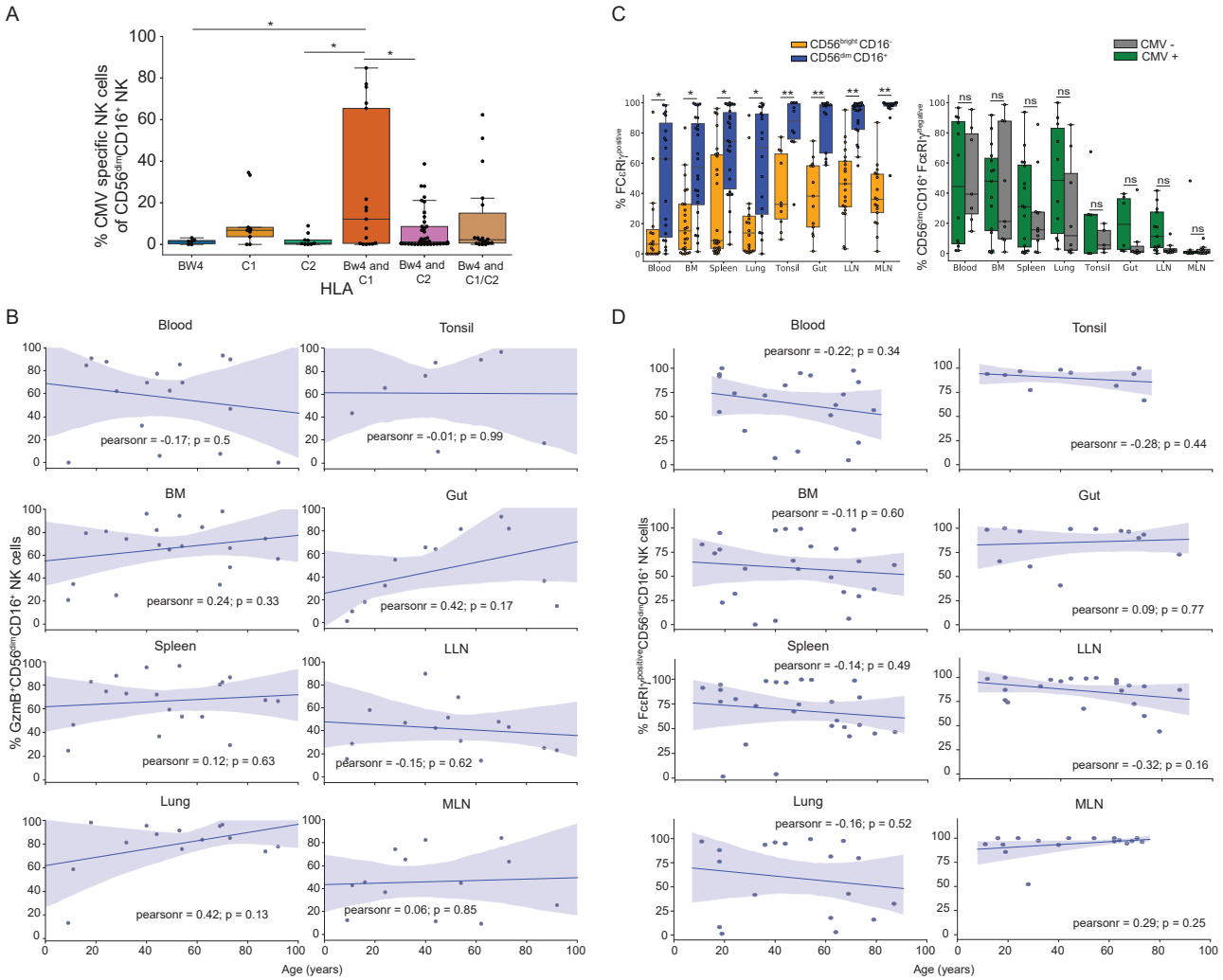

Figure S2. Distribution of NK Cell Functional Subsets Based on CMV Exposure and Age, Related to Figures 2 and 3

(A) Boxplot showing frequency of CMV-responsive ($CD56^{dim}CD16^{+}CD57^{+}NKG2C^{+}$) NK cells compiled from blood, BM, spleen, and lung from donors of indicated HLA types.

(B) Scatterplots showing the line of best fit for the frequency of $GzmB^{+}CD56^{dim}CD16^{+}$ NK cells in each tissue site as a function of age; pearsonr indicates the Pearson correlation coefficient for the comparison.

(C) Boxplot of compiled data from 10-24 donors showing the distribution of FcεRIγ-expressing NK cell subsets in different sites (left), and the frequency of $FcεRIγ^{negative}CD56^{dim}CD16^{+}$ NK cells between CMV -seronegative and -seropositive donors in different sites (right). $^{**}p \leq 0.01$, $^{*}p \leq 0.05$; ns, non-significant.

(D) Scatterplots showing the line of best fit for the frequency of $FcεRIγ^{+}CD56^{dim}CD16^{+}$ NK cells in each tissue site as a function of age; pearsonr indicates the Pearson correlation coefficient for the comparison.

Dots on the boxplots show data collected for each individual donor. BM, bone marrow; LLN, lung draining LN; MLN, mesenteric LN.

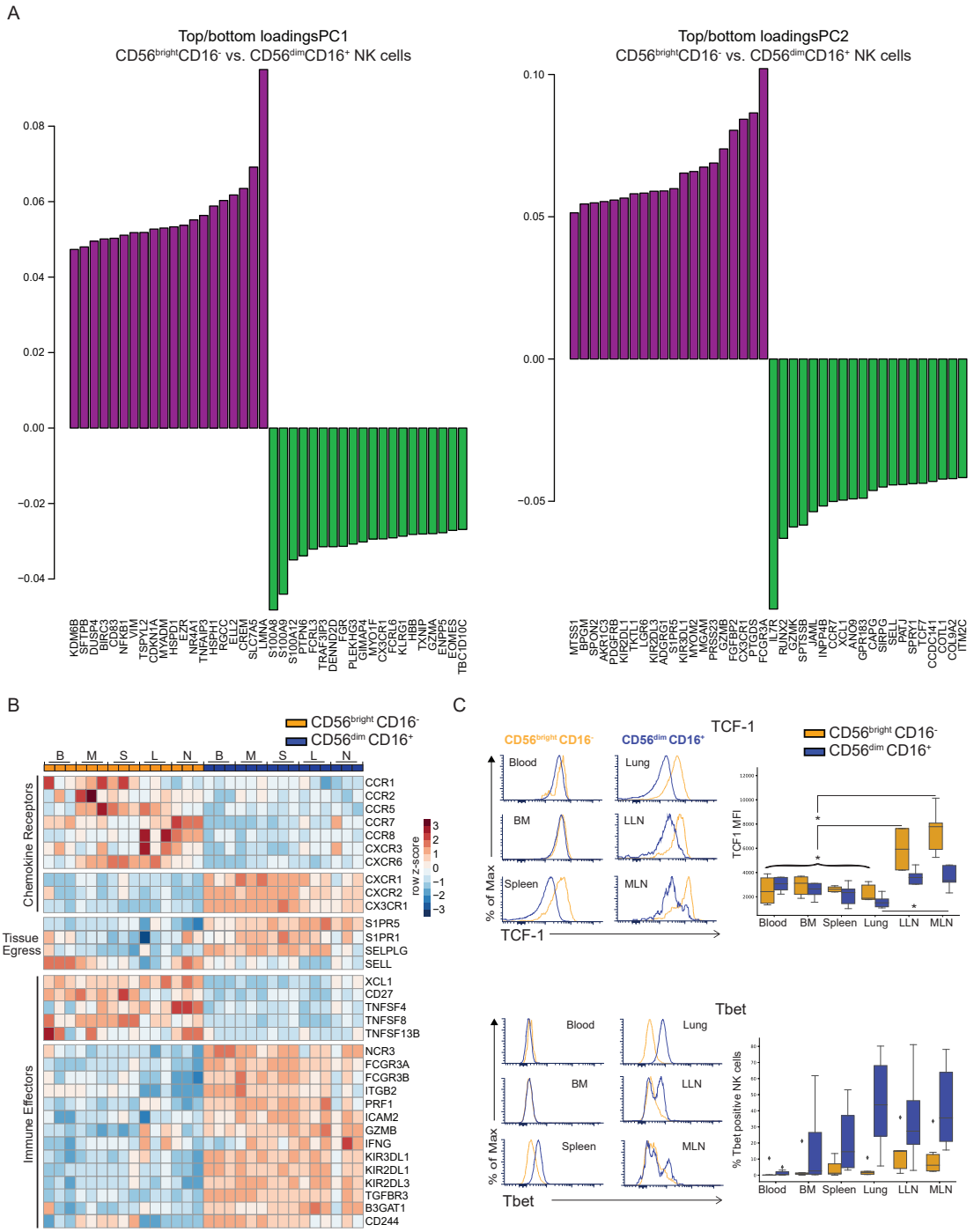

Figure S3. Differential Expression of Genes and Transcription Factors between CD56^{bright}CD16^{-} and CD56^{dim}CD16^{+} NK Cells, Related to Figure 4

(A) Bar plots showing highest/lowest loadings of principal component 1 and principal component 2 for PCA analysis comparing the global transcriptome of CD56^{bright}CD16^{-} and CD56^{dim}CD16^{+} NK cells in Figure 4A.

(B) Heatmap showing the differential expression of selected genes between CD56^{bright}CD16^{-} and CD56^{dim}CD16^{+} NK cell subsets isolated from 5 sites (B = Blood, M = Bone marrow, S = Spleen, L = Lung and N = LLN) from 3 donors.

(C) Representative histograms and boxplot of compiled data from 5 donors showing TCF1 (top) and Tbet (bottom) expression in NK cells subsets in different anatomical sites.

*p $\leq$ 0.05. Diamonds represent outliers in the data. BM, bone marrow; LLN, lung draining LN; MLN, mesenteric LN.

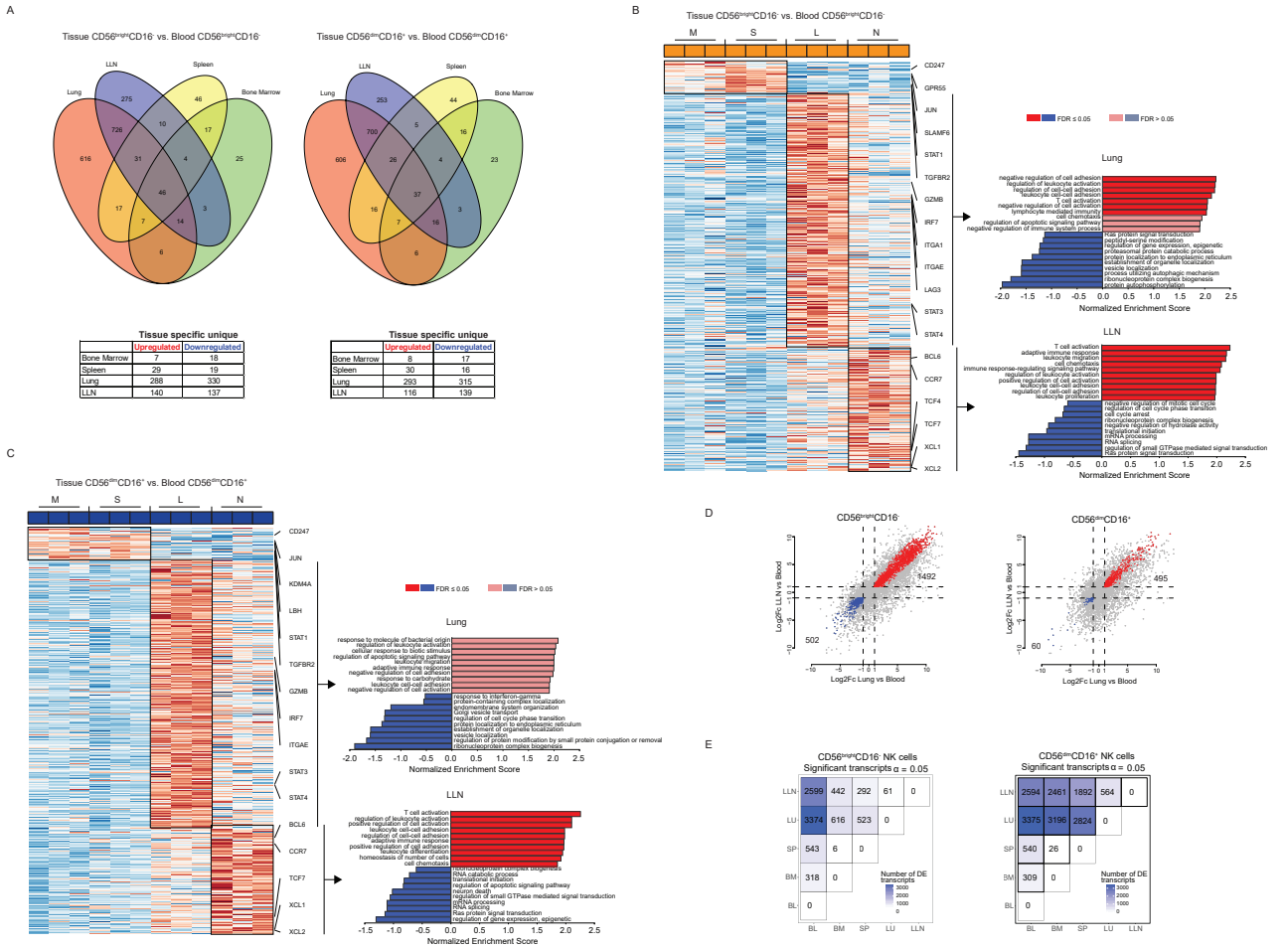

Figure S4. Tissue-Specific Transcriptional Programs for CD56^{bright}CD16^{-} and CD56^{dim}CD16^{+} NK Cells, Related to Figure 4

(A) Venn diagrams identifying unique differentially expressed (DE) genes between tissue CD56^{bright}CD16^{-} and blood CD56^{bright}CD16^{-} NK cells (top left) and tissue CD56^{dim}CD16^{+} and blood CD56^{dim}CD16^{+} NK cells (top right); table shows unique upregulated and downregulated genes for tissue CD56^{bright}CD16^{-} NK cells (bottom left) and tissue CD56^{dim}CD16^{+} NK cells (bottom right).

(B) *Left:* Heatmap shows upregulated genes in CD56^{bright}CD16^{-} NK cells in indicated sites. *Right*: graph shows pathways enriched in Lung and LLN CD56^{bright}CD16^{-} NK cells determined by GSEA. See Table S4.

(C) *Left:* Heatmap shows upregulated genes in CD56^{dim}CD16^{+} NK cells in indicated sites. *Right:* graph shows pathways enriched in Lung and LLN CD56^{dim}CD16^{+} NK cells determined by GSEA. See Table S5.

(D) Bi-plots for $\log_2$fold change (Fc) in gene expression for lung versus blood and LLN versus blood CD56^{bright}CD16^{-} NK cells (top) and lung versus blood and LLN versus blood CD56^{dim}CD16^{+} NK cells (bottom). Red dots represent genes similarly upregulated in both lung and LLN NK cell subsets (number in top right quadrant) and blue dots represent genes similarly downregulated in both lung and LLN NK cell subsets (number in bottom left quadrant).

(E) Matrix for the tissue wise comparison of transcriptional profile of CD56^{bright}CD16^{-} NK cells top and CD56^{dim}CD16^{+} NK cells bottom. Numbers in each box correspond to number of differentially expressed genes for each comparison. BL, blood; BM, bone marrow; SP, spleen; LU, lung; LLN, lung draining LN.

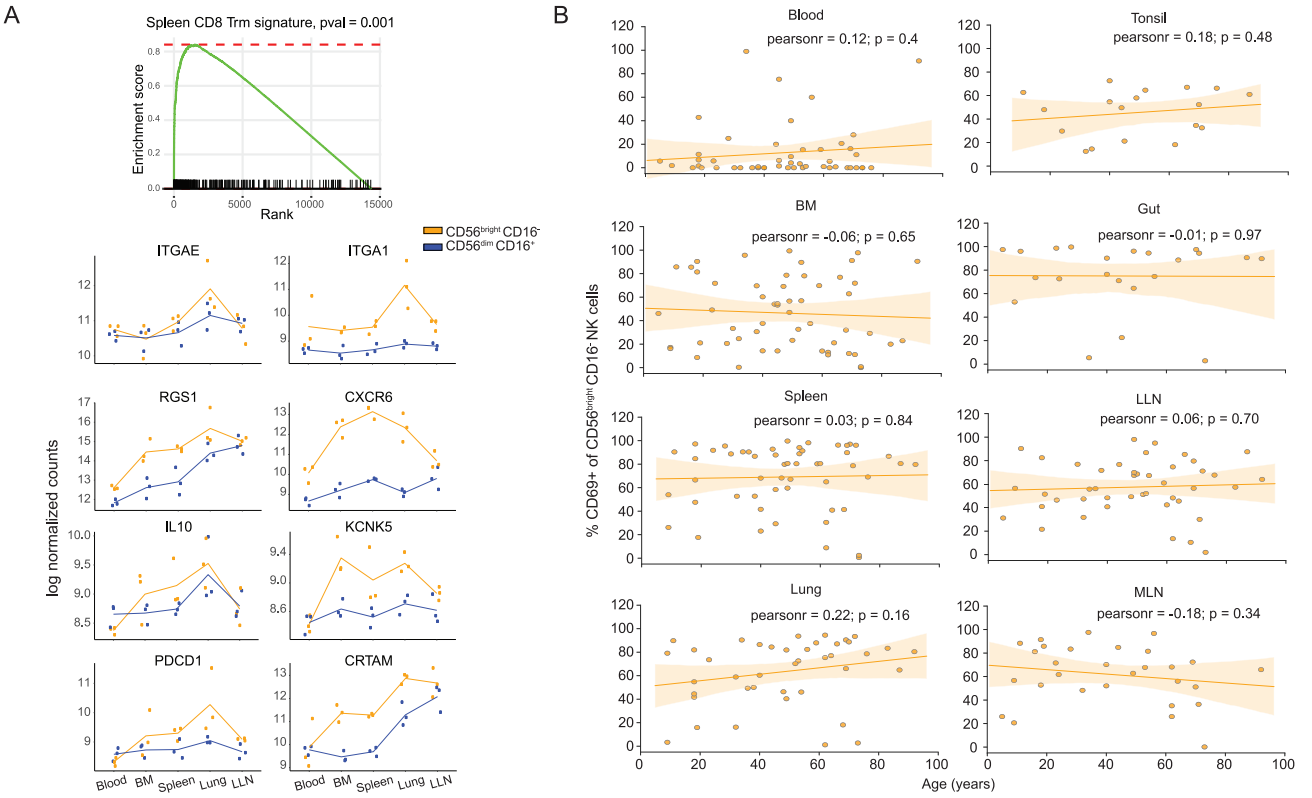

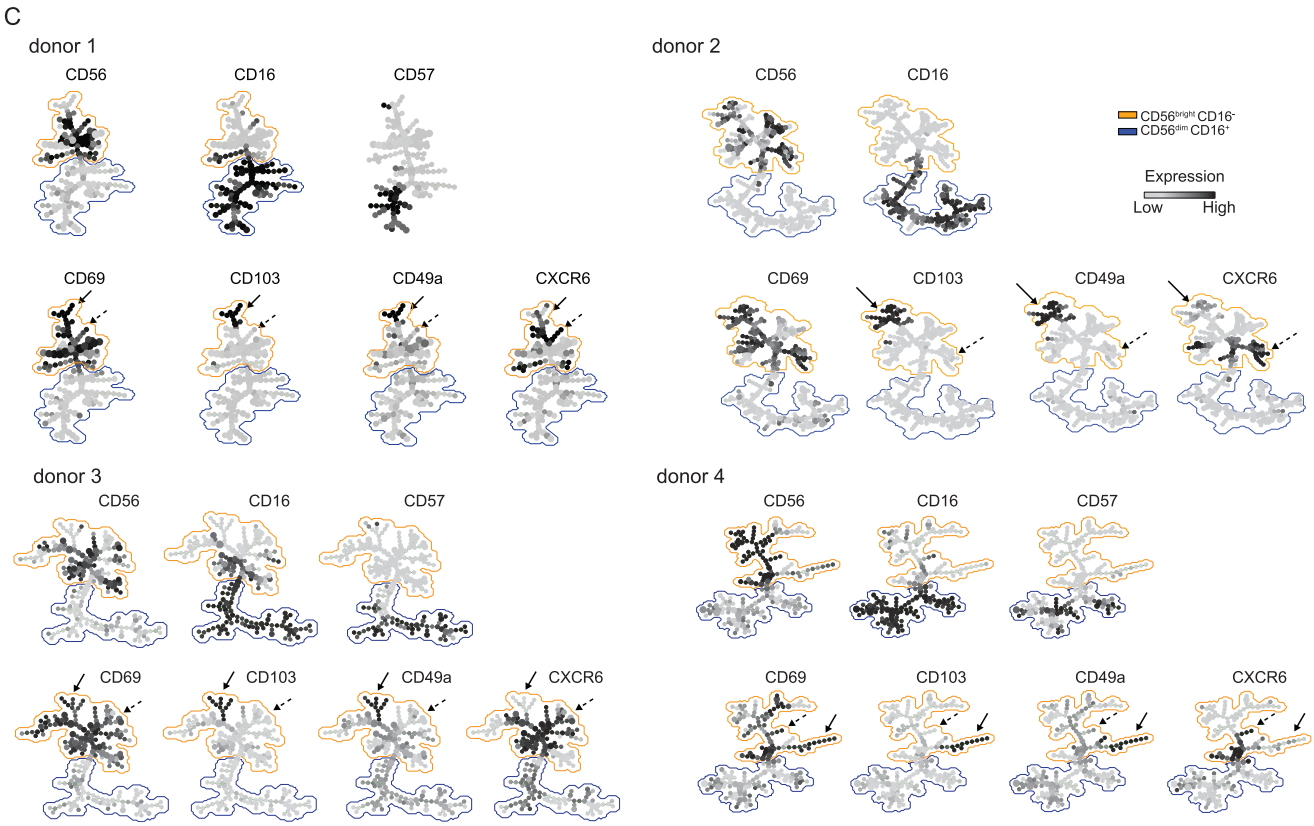

(legend on next page)

Figure S5. Transcriptional and Phenotypic Analysis of Tissue-Resident NK Cells in Different Sites, Related to Figures 5 and 6

(A) GSEA plot showing the enrichment of spleen CD8 tissue resident-memory T (Trm) gene signature within $CD56^{bright}CD16^{-}$ NK cells from all tissue sites (top) and scatterplots showing log normalized counts of key tissue-residence genes shown in Figure 5B heatmap (bottom). Dots show data for each individual sample and the line connects the mean value for each group of samples.

(B) Scatterplots showing the frequency of $CD69^{+}CD56^{bright}CD16^{-}$ NK cells in each tissue site as a function of age and line of best fit between the variables, pearsonr indicates the Pearson correlation coefficient for the comparison.

(C) Heterogeneity of trNK cells. SPADE plots for NK cells isolated from blood, BM, spleen, lung, gut, LLN, and MLN (donor 1) and from blood, BM, spleen, lung, and LLN for 3 additional donors (donors 2, 3, and 4). Solid black arrow identifies $CD103^{+}$ $CD49^{+}$ NK cells and dashed black arrow identifies $CXCR6^{+}$ NK cells. BM, bone marrow; LLN, lung draining LN; MLN, mesenteric LN

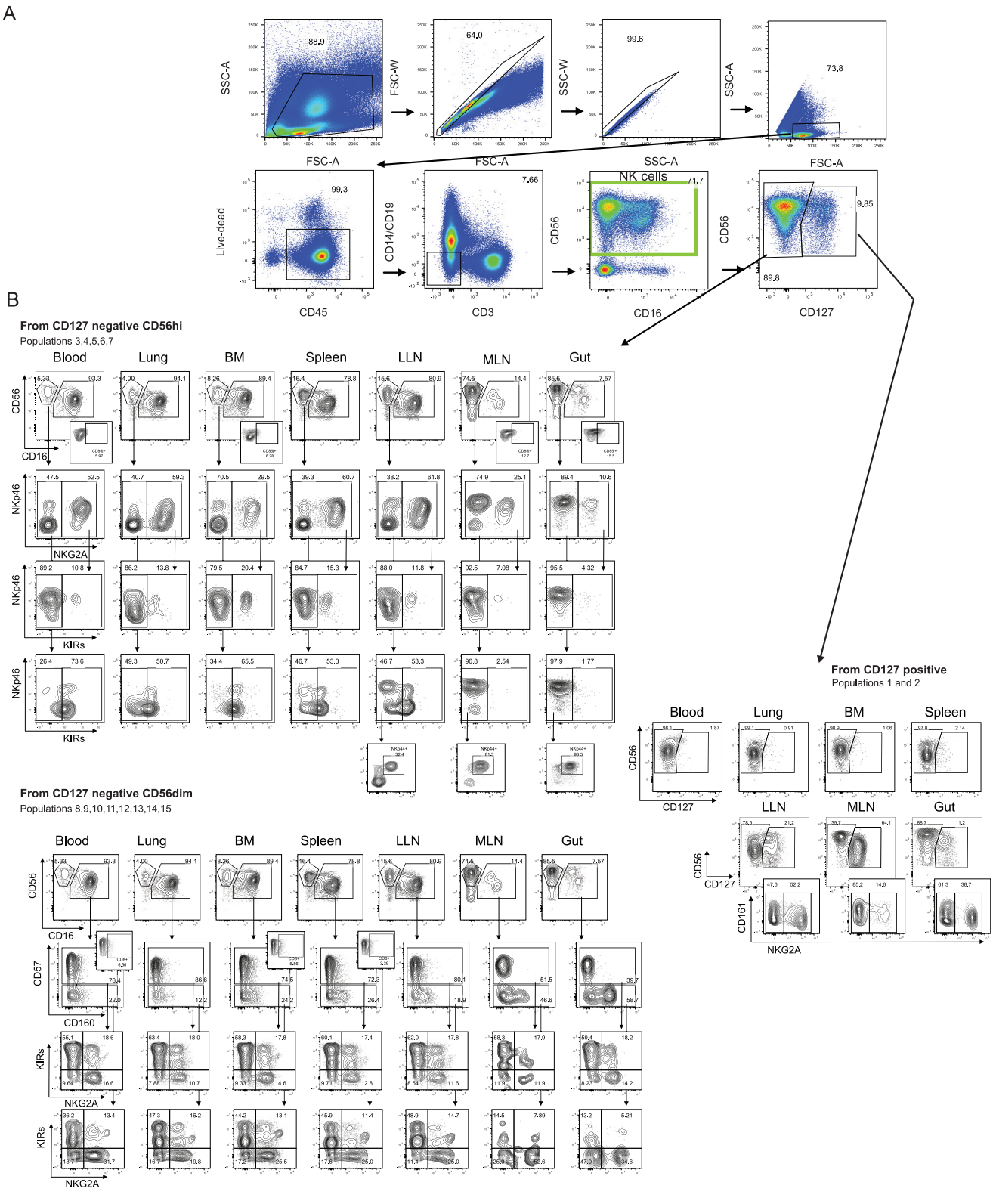

(legend on next page)

Figure S6. Gating Strategy and Representative Flow Plots for Clusters Identified by High-Dimensional Flow Cytometry Analysis, Related to Figure 7

(A) NK cells were identified as SSC-A^{low}CD45^{+}CD14^{-}19^{-}CD3^{-}CD56^{+} cells and used to carry out further analysis as described in materials and methods.

(B) Representative flow plots showing the expression of markers on NK cell clusters identified by high-dimensional analysis. BM, bone marrow; LLN, lung draining LN; MLN, mesenteric LN.

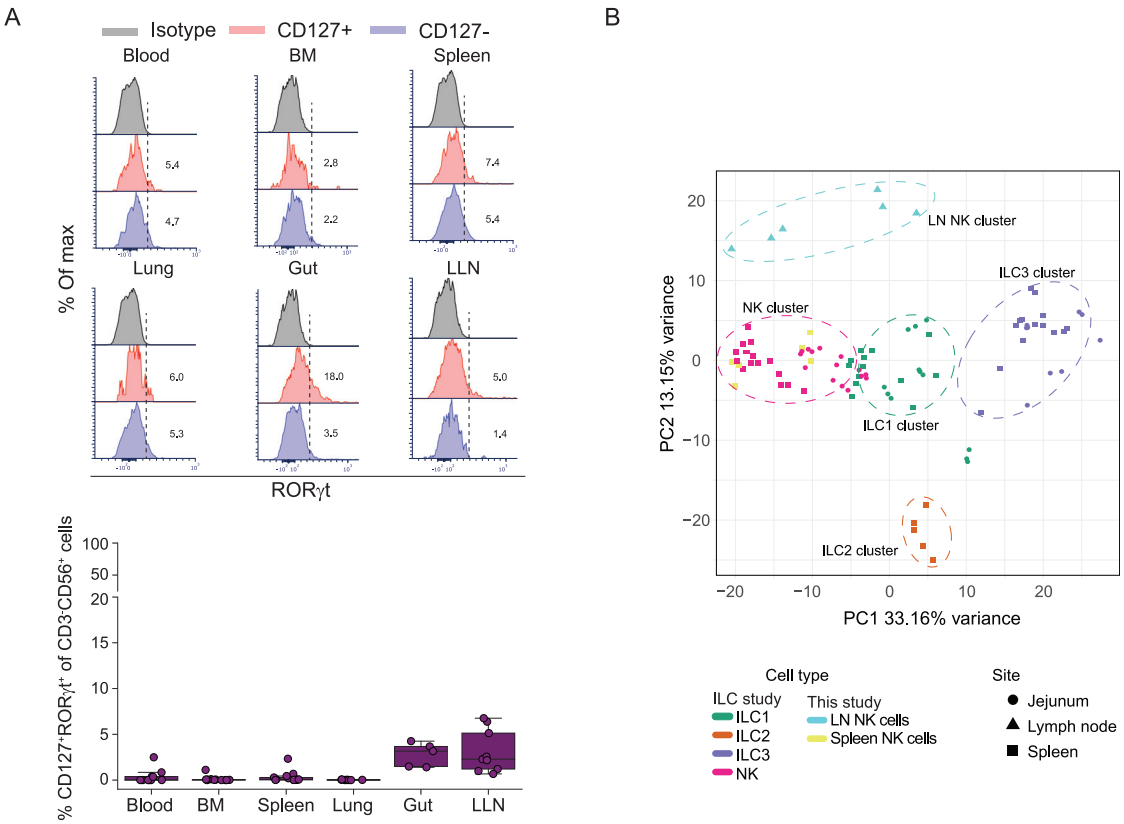

Figure S7. CD56^{bright}CD16^{-} NK Cells in Tissues Are Phenotypically and Transcriptionally Distinct from Known ILC Subsets, Related to Figure 7

(A) Representative histograms showing the expression of RORγt on CD127^{+} and CD127^{-} cells in blood and tissue sites on top, and on bottom boxplot showing the frequency of CD127^{+}RORγt^{+} cells of the total CD3^{-}CD56^{+} cells in blood and tissue sites compiled from 5-13 donors.

(B) PCA plot showing comparison of the transcription profile of NK cells from spleen (golden squares) and LLN (cyan triangles) from this study and NK cells and ILC subsets from spleen and jejunum from the ILC study (Yudanin et al., 2019). BM, bone marrow; LLN, lung draining LN; MLN, mesenteric LN.